Research Article Vol. 9, No. 9 / September 2021 / Photonics Research 1865

PHOTONICS Research

Generating heralded single photons with a switchable orbital angular momentum mode

Shan Zhang, Shikang Li, Xue Feng,* Kaiyu Cui, Fang Liu, Wei Zhang, and Yidong Huang

Department of Electronic Engineering, Tsinghua University, Beijing 100084, China
**Corresponding author: x-feng@tsinghua.edu.cn*

Received 20 May 2021; revised 8 July 2021; accepted 17 July 2021; posted 20 July 2021 (Doc. ID 432035); published 31 August 2021

The orbital angular momentum (OAM) carried by photons defines an infinitely dimensional discrete Hilbert space. With OAM modes, high-dimensional quantum states can be achieved for quantum communication and cryptography. Here we demonstrate a heralded single-photon source with a switchable OAM mode, which consists of a heralded single-photon source and an integrated OAM emitter as the mode converter. As the first step, the heralded single-photon source is based on the dispersion-shifted fiber. In this work, the OAM mode (quantized by topological charge l) carried by the heralded single photon (at fixed wavelength of 1555.75 nm) can be switched within the range of $l = 3$–7 while the mode purity is more than 80%.

https://doi.org/10.1364/PRJ.432035

1. INTRODUCTION

Orbital angular momentum (OAM) is an independent degree of freedom (DoF) associated with the helical phase fronts of optical vortex beams, and such azimuthal phase distribution can be described by the topological charge l with infinite dimensionality [1]. In classical optical communication, the optical information encoding density and processing capability could be significantly improved with the OAM mode [2–4]. Moreover, the detection [5–7] and generation of OAM beams have developed considerably. Among previous proposals, a light beam with an OAM mode can be generated through the spiral phase plate [8], metasurface [9–11], or spatial light modulator (SLM) [12]. With continuous growth of communication capacity and device complexity, an integrated light source is highly desired for optical communication and information processing [13,14]. To explore and utilize the high-dimensional property, many efforts have been made to generate a switchable OAM mode on-chip [15,16].

In quantum optics, OAM has been demonstrated as a promising platform for high-dimensional quantum entanglement [17] and quantum key distribution [18–20]. Additionally, heralded single photons with the OAM mode could be applied on quantum ghost imaging, benefiting from the correlation between photon pairs and the spatial angle sensitivity of the OAM mode [21,22]. Generally, the quantum state with the OAM mode can be generated by spontaneous parametric down conversion (SPDC) in nonlinear crystals [23–25] or transformed from other DoFs [26], which are based on bulky spatial optical systems and are hard to be expanded. In the latest research, an integrated single-photon source with the OAM mode is proposed by combining the quantum dot and an integrated OAM emitter [27], where the topological charge of the OAM mode is fixed and nonadjustable. Until now, there has still been a practical problem left, i.e., how to dynamically switch the topological charge carried by the single photon of fixed wavelength.

In this paper, we propose and demonstrate a quantum light source with a switchable OAM mode based on a heralded single-photon source and an integrated OAM emitter as the mode converter. The heralded single-photon source is based on the spontaneous four-wave mixing (SFWM) of dispersion-shifted fiber (DSF) [28]. By uncoupling the OAM emitter and quantum light source, the topological charge can be switched dynamically by manipulating the OAM emitter without disturbing the quantum light source. Here, the design of the integrated OAM emitter is based on our previous work [16], and the topological charges of the emitted OAM modes are increased to the range of −10 to +10. With this configuration, the heralded single photon with a switchable OAM mode can be generated and measured at a fixed wavelength. For single-photon states, the topological charges are switched within the range of $l = 3$–7, while the mode purity is more than 80%. The measured coincidence counts and coincidence counts-to-accidental coincidence counts ratio (CAR) have ranges of 24–32 and 6.20–10.18, respectively. Such results indicate that the heralded single photon with a switchable OAM mode has been generated successfully. It should be mentioned that such a configuration could be further modified to realize a fully integrated quantum OAM mode state emitter with a heralded single-photon source based on a silicon wire waveguide [29]. We believe that this work could provide a flexible and scalable platform for achieving a quantum state with a switchable OAM mode,

which can serve as a quantum light source for high-dimensional quantum applications and boost the application of the OAM mode in quantum optics.

2. DESIGN OF THE HERALDED SINGLE-PHOTON SOURCE WITH A SWITCHABLE OAM MODE

To generate the heralded single photon with the OAM mode, a heralded single-photon source combined with an OAM emitter as the mode converter is proposed in this work. Based on the SFWM process, the laser pumped nonlinear optical media, DSF here, could generate time-energy correlated photon pairs randomly [28]. This effect provides a method to generate a heralded single-photon state with the help of postselection. The photon pairs can be separated according to their wavelength, while one photon (the heralding photon) of the photon pair is detected by a detector, indicating that the other one (the heralded photon) is a single photon that could be utilized. In this work, such a heralded single photon is converted to the OAM mode by an OAM emitter without destroying the time-correlated feature of photon pairs. Through an appropriate detection method, the coincidence counts analyzed by time-correlated single-photon counts (TCSPCs) would demonstrate the successful generation of the heralded single photon with the OAM mode.

As shown in Fig. 1, with DSF pumped by a pulse laser (40 MHz), the photon pairs are generated through SFWM and then divided by a dense wavelength-division multiplexer (DWDM). Here, the idler and signal photons serve as the heralding and heralded photon, respectively. The idler photons are directly detected by the single-photon avalanche diode (SPAD), while the signal photons are coupled into the OAM emitter so that they can be converted to the OAM mode. Since the employed SPAD is packaged with a single-mode fiber (SMF) pigtail, the heralded photons with OAM modes have to be converted to fundamental Gaussian mode by SLM combined with some additional wave plates and a mirror. Moreover, this part of the spatial optical system would also be employed to characterize the OAM emitter, which will be introduced in detail in the next section.

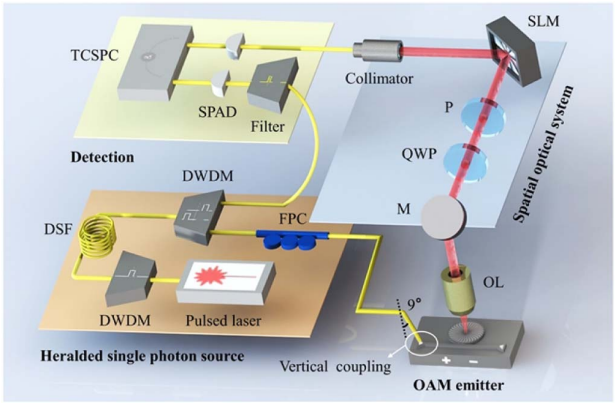

Fig. 1. Experimental scheme consisting of the heralded single-photon source, OAM emitter, spatial optical system, and detector. FPC, fiber polarization controller; OL, objective lens; M, mirror; QWP, quarter-wave plate; P, polarizer.

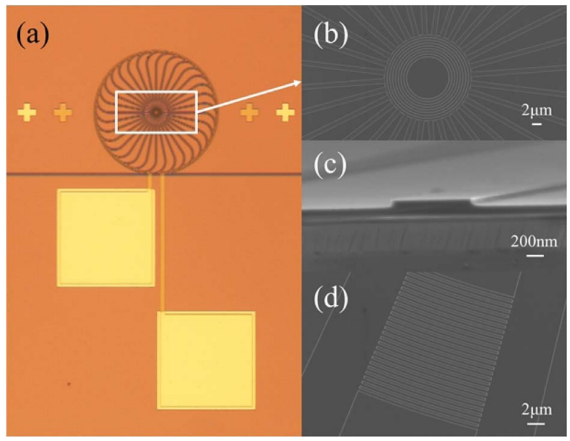

Fig. 2. (a) Microscopic photograph of the OAM emitter; (b) scanning electron microscopy (SEM) image of the concentric scattering grating in the center of the OAM emitter; SEM images of (c) the shallow ridge waveguide and (d) the grating for vertical coupling.

The employed OAM emitter is shown in Fig. 2(a). Following the design of our previous work [16], the emitter consists of a bus waveguide, a microring cavity, 32 download waveguides, and a concentric scattering grating. The principle of this emitter depends on the equally distributed download waveguides to extract whispering gallery mode (WGM) in the microring cavity. Through this process, the WGM with intrinsic azimuthal phase gradient is coupled into the concentric scattering grating, shown in Fig. 2(b), and then scattered into free space, indicating the spatial OAM mode. The radius of microring cavity is designed as 200 μm so that a wider range of topological charge can be achieved. To reduce the transmission loss, the emitter is designed and fabricated by a shallow ridge waveguide, as illustrated in Fig. 2(c). Here, silicon-on-insulator (SOI) with a top thickness of silicon equaling 220 nm is employed. The etching depth and width of ridge waveguide are 70 nm and 1 μm, respectively. To couple the signal photons into the OAM emitter, vertical coupling is employed; the structure is shown in Fig. 2(d).

Furthermore, the titanium electrode is deposited on the top of the microring cavity to tune the refractive index of the waveguide by thermo-optic effect [30]. As shown in Fig. 2(a), two yellow squares are aluminum bonding pads connected to the titanium electrodes. There are two considerations to introduce this thermo-optic controller. First, the resonant wavelength of the microring cavity (or the operation wavelength of the OAM emitter) can be tuned to align with the signal-photon wavelength of the heralded source. Second, for fixed incident wavelength, the topological charge of the OAM mode can be dynamically switched. Thus, the thermo-optic controller is very crucial to achieving a heralded single-photon source with the OAM mode.

3. CHARACTERIZATIONS OF THE OAM EMITTER

First, the fabricated OAM emitter is characterized by a tunable laser (SANTEC TSL-710) instead of the heralded single-photon source while the emission is detected by a charge-coupled device (CCD) camera or an optical power meter

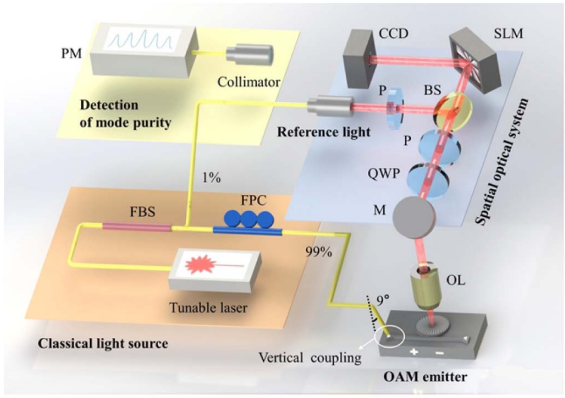

Fig. 3. Experimental setup for measuring the topological charge and mode purity. BS, beam splitter; FBS, fiber beam splitter.

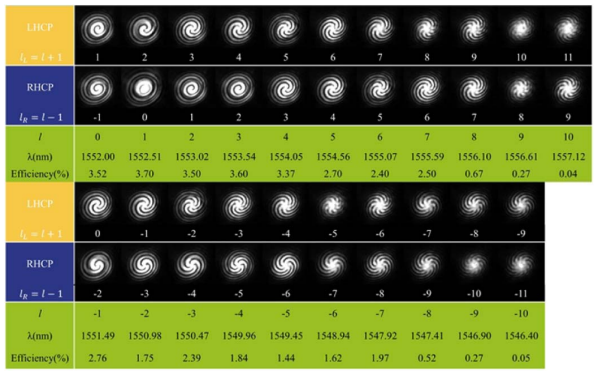

Fig. 4. Interference fringes of Gaussian mode and generated OAM modes of l ranging between −10 and +10 under different incident wavelengths. Each OAM mode could be decomposed to an LHCP part and an RHCP part corresponding to two rows of interference patterns. The conversion efficiency of different OAM modes is also shown at the bottom.

(PM), as shown in Fig. 3. To identify the topological charge of the generated OAM, the incident laser power is divided into two parts, while 99% of it is coupled into the OAM emitter through vertical coupling and 1% is directly guided to the spatial optical system as a reference light of Gaussian mode. After generated by the emitter and collected into the spatial optical system, the generated OAM beam would interfere with the reference light, and the CCD camera would record the interference patterns that reveal topological charge [31]. Here, the SLM is settled as a mirror.

With our proposed OAM emitter, the generated OAM mode is azimuthally polarized as discussed in Ref. [16] and could be decomposed into two spin components as

$$\begin{pmatrix} -\sin\varphi \\ \cos\varphi \end{pmatrix} e^{-il\varphi} = -\frac{i}{2}\begin{pmatrix} 1 \\ i \end{pmatrix} e^{-i(l+1)\varphi} + \frac{i}{2}\begin{pmatrix} 1 \\ -i \end{pmatrix} e^{-i(l-1)\varphi}, \tag{1}$$

where φ is the azimuthal angle in the cylindrical coordinate system and i is the unit imaginary number. The right side in Eq. (1) stands for the left-handed circularly polarized (LHCP) part with topological charge of $l_L = l + 1$ and right-handed circularly polarized (RHCP) part with topological charge of $l_R = l - 1$. Hence, in the spatial optical system, the quarter-wave plate (QWP) and polarizer are introduced to extract one of the spin components and rotated to linear polarization for subsequent interference with the linearly polarized reference beam. Each spin component could be the reference to identify the topological charge l of the generated OAM mode [32]. For example, if $l_L = 2$ and $l_R = 0$, then $l = 1$ can be confirmed. Figure 4 shows the measured interference patterns of the generated OAM modes, and the topological charges of the azimuthally polarized OAM range from −10 to +10, corresponding to incident wavelengths from 1546.40 to 1557.12 nm. The wavelength interval of the two adjacent modes is ∼0.5 nm, corresponding to the free spectral range (FSR) of the WGM. For each OAM mode, there are two interference patterns corresponding to the LHCP and RHCP state, respectively, and they together confirm the topological charges of the generated OAM modes. Furthermore, the conversion efficiency of different OAM modes is measured, as shown in Fig. 4. The conversion efficiency is defined as $\frac{P_{\text{emission}}}{P_{\text{input}}}$, where P_{input} is the light power coupled into the OAM emitter, and P_{emission} is that of the generated OAM mode. In our experiment, P_{input} is obtained by subtracting the loss of vertical coupling from the incident light while P_{emission} is measured by a PM settled before the QWP in the spatial optical system and subtracted by the loss of OL.

As mentioned above, the topological charge of the generated OAM mode could be switched through applying electrically driving power on the thermo-optic controller to change the refractive index of the waveguide. Here, the wavelength of incident laser is fixed at 1554.56 nm, corresponding to the $l = +5$ azimuthally polarized OAM mode with a driving voltage of 0 V. By increasing the driving voltage, the resonant wavelength of the microring cavity would be redshifted, and the topological charge would decrease. In Fig. 5, the red line shows the linear relation between topological charges and electrically driving power, together with the blue line, which corresponds to the quadratic relation between topological charges and electrically driving voltage. There are 11 OAM modes switched within the driving voltage ranging between 0 and 61.5 V, and their topological charges can be confirmed by the interference fringes (shown in insets) of the LHCP state as $l = l_L - 1$. It should be mentioned that this result is limited by the maximum voltage of the utilized electrical power source (61.5 V). Actually, a

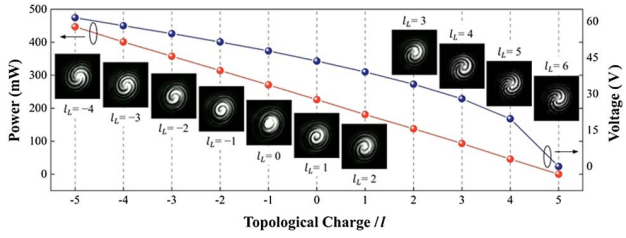

Fig. 5. Relation between the topological charges and the electrically driving power (red marks), together with the corresponding driving voltage (blue marks), while the incident wavelength is fixed at 1554.56 nm. The insets are the interference fringes corresponding to each OAM mode of the LHCP state.

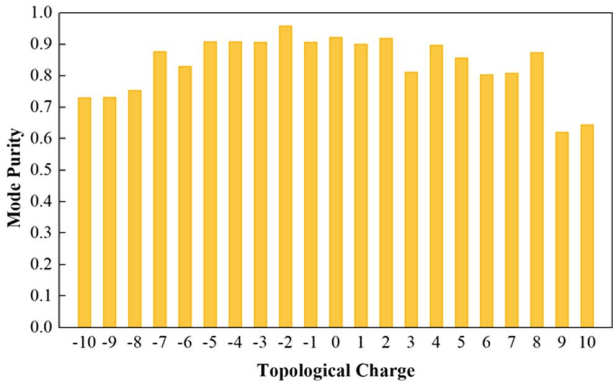

Fig. 6. Mode purities of azimuthally polarized OAM modes with l ranging between −10 and +10.

wider switching range could be achieved through a higher driving voltage and an optimized design of the electrode.

Furthermore, the mode purities of azimuthally polarized OAM modes are also quantitatively analyzed by a method similar to the tomography [5]. Actually, the mode purity and scattering efficiency of concentric scattering grating mainly determine the conversion efficiency of the OAM emitter. According to the Nyquist sampling theorem, the emitter with 32 download waveguides could generate OAM modes with topological charges ranging between −15 and +15 theoretically. Hence, the mode purity of the OAM mode with topological charge of l is defined as $\frac{P_l}{\sum_{m=-15}^{15} P_m}$. Here, $P_x(x = m/l)$ represents the intensity of the OAM mode with a topological charge of x. For this measurement, the CCD camera in Fig. 3 is replaced by a PM combined with a collimator, and the beam splitter (BS) is removed. The SLM is programmed with varying phase masks of helical phase gradient, and the topological charges (denoted as m) range between −15 and +15. Only for $m = -l$, could the SLM exactly compensate for the phase fronts of the generated OAM mode to the planar phase fronts, indicating a fundamental Gaussian mode. Then a collimator would couple this Gaussian mode to an SMF with an optical PM in the end to detect the corresponding power. Moreover, the collimator also serves as a filter, only detecting the fundamental Gaussian mode. The measured mode purities of generated OAM modes within the range of l = −10 to +10 are shown in Fig. 6. For each mode, the RHCP and LHCP OAM states are measured, and the final result is the average of these two values. It can be seen that most measured mode purities are more than 80%, and this result is stable for all fabricated samples.

4. COINCIDENCE COUNTS OF HERALDED SINGLE-PHOTON SOURCE WITH AN OAM MODE

For a heralded single-photon source, the photon pairs are generated by SFWM in DSF. A pulsed laser (1552.5 nm) is coupled into a 500 m DSF in liquid nitrogen; then the signal and idler photons with wavelength of 1555.75 nm and 1549.32 nm are filtered out by DWDM, and the pump photons are blocked simultaneously. Following polarization adjustment, signal photons are coupled into the OAM emitter, whose operation wavelength is tuned to align with the wavelength of signal photons (1555.75 nm). To certify the generation of the heralded single photon with the OAM mode, the coincidence counts between the heralded single photons with the OAM mode and the heralding photons are measured with the help of the SLM. Here, the OAM mode should also be converted to Gaussian mode by the SLM, as discussed above, and only the first-order diffraction is collected after the SLM and coupled into SPAD. It needs to be emphasized that, after being modulated by the OAM emitter, the bandwidth of signal photons would shrink to ∼0.05 nm, which is determined by the full width at half-maximum (FWHM) of the microring cavity. Correspondingly, an additional filter with bandwidth of 0.1 nm is introduced for idler photons to avoid the detector saturation.

The typical coincidence counts corresponding to $l = 5$ of the RHCP state are shown in Fig. 7(a). Within 30 min, the maximum coincidence counts are 32. Moreover, the topological charges of the OAM modes can be switched within the range of $l = 3$–7 by tuning the driving voltage ranging between 12 V and 45 V. The coincidence counts (30 min) and CAR of the RHCP OAM states are shown in Fig. 7(b), corresponding to the blue and yellow marks, respectively. CAR is a good figure of merit to evaluate the time correlation and is defined as CAR $= \frac{N_{cc}}{N_{acc}}$, where N_{cc} is the coincidence counts and N_{acc} is the accidental coincidence counts. With the result of CAR > 1, the time correlation can be confirmed [33–35]. Actually, N_{acc} mainly comes from the dark counts of SPAD and noises in the SFWM process in DSF. When calculating the CAR, N_{acc} is defined as the average of 20 values evenly distributed on the right and left sides of the peak value, and the time delay between the adjacent values is 25 ns. Here the coincidence counts are 24–32 for $l = 3$–7, and this result is mostly limited by the conversion efficiency of the emitter and the detection loss. Nevertheless, it still can be clearly seen from Fig. 7 that the coincidence counts have proven the successful generation of a heralded single photon with the OAM mode. Theoretically, the efficiencies of the OAM emitter, the SLM, and the collimator would decrease as the topological charge increases, but these variations are negligible compared to the total loss. As shown in Fig. 7(b), there is no obvious relation between the topological charges and coincidence counts/CAR in the measurement range, and the data fluctuation mainly comes from the random error.

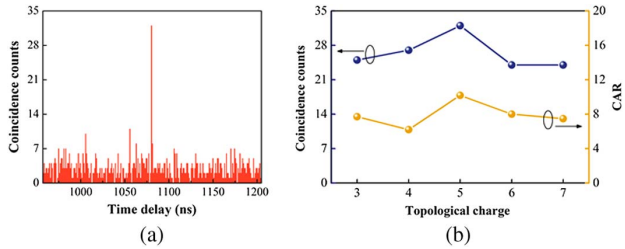

Fig. 7. (a) Typical coincidence counts of heralded single photons with an OAM mode of $l = 5$; coincidence counts and CAR of heralded single photons with OAM modes of $l = 3$–7.

5. DISCUSSION

In our experiment, the average power of pulsed laser is 0.4 mW to balance the trade-off between coincidence counts and CAR. In order to obtain higher single-photon state generation rates, CAR is sacrificed to 6.20–10.18. The single-side photon counts of the heralded single-photon source are ∼188,000 s^{-1} with the SPAD's detection efficiency of 25%. For idler photons, the single-side photon counts are ∼14,000 s^{-1} after the filter with bandwidth of 0.1 nm (insertion loss of ∼2.2 dB). For signal photons with different OAM modes ($l = 3$–7), the total loss from FPC to SPAD ranges from 40.4 to 41.5 dB, caused by the vertical coupling loss (∼7 dB), OAM conversion efficiency (2.4%–3.6%), objective lens collection efficiency (40%), wave plates insert losses (∼3.23 dB), loss of SLM modulation (4.13–4.3 dB), coupling loss of collimator (3.47–5.07 dB), and some other transmission dissipation (∼3.03 dB). Additionally, filtered by the OAM emitter (FWHM of 0.05 nm), the single side photon counts of the heralded photons are finally estimated as 0.83–1.07 s^{-1}, which is much lower than the dark counts (∼99 s^{-1}). Since there is no time correlation of dark counts between two SPADs, the dark counts would only induce low accidental coincidence counts. In our experiment, the average value of accidental coincidence counts is about 3–4.36 (30 min). Therefore, the coincidence counts and CAR could confirm the successful emission of a heralded single photon with the OAM mode.

Actually, the final coincidence counts are affected not only by the generation rates of the heralded single photon with the OAM mode but also the method of detection. Here, the losses induced by detection are ∼15.7 dB so that relatively low coincidence counts are achieved. Actually, the coincidence counts could reach ∼1190 (30 min) without the detection loss. From the perspective of merely considering the heralded single photon with the OAM mode, the generation rates are mainly determined by both the generation rates of the heralded single-photon source and the conversion efficiency of the OAM emitter. Additionally, the vertical coupling structure is adopted between the heralded single-photon source and the OAM emitter to simplify the fabrication and experimental process at a cost of 7 dB loss. This coupling loss could be alleviated by horizontal coupling. Moreover, the photon pairs could be generated in bus waveguide [29] or microring cavity [36] directly, since SFWM could also occur in a silicon waveguide as well. In that case, a fully integrated heralded single-photon source with a switchable OAM mode could be achieved, which has lower coupling loss and higher stability. We are still working on it.

Thanks to the spatial separation of the heralded single-photon source and the OAM emitter, we can utilize the thermo-optic effect to switch the topological charge of the OAM mode without disturbing the cooling condition of the DSF. Theoretically, the topological charges of optical quantum OAM modes could reach −10 to +10, the same as the classical domain. Limited by the operation wavelength of a single-photon source and the driving voltage of power source, only $l = 3$–7 OAM modes are demonstrated in this work. Actually, a wider switchable range of topological charge could be achieved if cooling equipment is attached below the OAM emitter to tune the frequency shift in another direction.

6. CONCLUSION

In this work, a heralded single-photon source with a switchable OAM mode is demonstrated. We have designed and optimized an integrated OAM emitter to generate classical OAM modes with $l = -10$ to +10, and the mode purities have been tested experimentally. For optical quantum domain, the topological charges of the OAM modes can be switched between 3 and 7 through the thermo-optic effect, and all these OAM modes are generated with mode purity >80%. As the first step to realize an integrated quantum light source with a switchable OAM mode, we utilize the heralded single-photon source based on DSF. Actually, this scheme could be further modified by adopting a quantum light source based on a silicon waveguide. Our proposal could provide a flexible and scalable platform to generate a heralded single photon with a switchable OAM mode, namely, a high-dimensional quantum state, which promises to increase the information capacity of quantum communication and cryptography.

Funding. National Key Research and Development Program of China (2017YFA0303700, 2018YFB2200402); National Natural Science Foundation of China (61621064, 61875101); Beijing Innovation Center for Future Chip; Frontier Science Center for Quantum Information; Beijing Academy of Quantum Information Sciences; Tsinghua Initiative Scientific Research Program.

Acknowledgment. The authors would like to thank Mr. Sirui Yuan for valuable discussions and helpful comments.

Disclosures. The authors declare no conflicts of interest.

Data Availability. Data underlying the results presented in this paper are not publicly available at this time but may be obtained from the authors upon reasonable request.

REFERENCES

1. L. Allen, M. W. Beijersbergen, R. J. C. Spreeuw, and J. P. Woerdman, "Orbital angular momentum of light and the transformation of Laguerre-Gaussian laser modes," Phys. Rev. A **45**, 8185–8189 (1992).
2. J. Wang, J.-Y. Yang, I. M. Fazal, N. Ahmed, Y. Yan, H. Huang, Y. Ren, Y. Yue, S. Dolinar, M. Tur, and A. E. Willner, "Terabit free-space data transmission employing orbital angular momentum multiplexing," Nat. Photonics **6**, 488–496 (2012).
3. N. Bozinovic, Y. Yue, Y. Ren, M. Tur, P. Kristensen, H. Huang, A. E. Willner, and S. Ramachandran, "Terabit-scale orbital angular momentum mode division multiplexing in fibers," Science **340**, 1545–1548 (2013).
4. Y. Yan, G. Xie, M. P. J. Lavery, H. Huang, N. Ahmed, C. Bao, Y. Ren, Y. Cao, L. Li, Z. Zhao, A. F. Molisch, M. Tur, M. J. Padgett, and A. E. Willner, "High-capacity millimetre-wave communications with orbital angular momentum multiplexing," Nat. Commun. **5**, 4876 (2014).
5. J. Leach, M. J. Padgett, S. M. Barnett, S. Franke-Arnold, and J. Courtial, "Measuring the orbital angular momentum of a single photon," Phys. Rev. Lett. **88**, 257901 (2002).
6. G. Gibson, J. Courtial, M. J. Padgett, M. Vasnetsov, V. Pas'ko, S. M. Barnett, and S. Franke-Arnold, "Free-space information transfer using light beams carrying orbital angular momentum," Opt. Express **12**, 5448–5456 (2004).

7. G. C. G. Berkhout, M. P. J. Lavery, J. Courtial, M. W. Beijersbergen, and M. J. Padgett, "Efficient sorting of orbital angular momentum states of light," Phys. Rev. Lett. **105**, 153601 (2010).
8. K. Sueda, G. Miyaji, N. Miyanaga, and M. Nakatsuka, "Laguerre-Gaussian beam generated with a multilevel spiral phase plate for high intensity laser pulses," Opt. Express **12**, 3548–3553 (2004).
9. L. Marrucci, C. Manzo, and D. Paparo, "Optical spin-to-orbital angular momentum conversion in inhomogeneous anisotropic media," Phys. Rev. Lett. **96**, 163905 (2006).
10. R. C. Devlin, A. Ambrosio, N. A. Rubin, J. P. B. Mueller, and F. Capasso, "Arbitrary spin-to–orbital angular momentum conversion of light," Science **358**, 896–901 (2017).
11. R. Dharmavarapu, K. Izumi, I. Katayama, S. H. Ng, J. Vongsvivut, M. J. Tobin, A. Kuchmizhak, Y. Nishijima, S. Bhattacharya, and S. Juodkazis, "Dielectric cross-shaped-resonator-based metasurface for vortex beam generation at mid-IR and THz wavelengths," Nanophotonics **8**, 1263–1270 (2019).
12. A. Forbes, A. Dudley, and M. McLaren, "Creation and detection of optical modes with spatial light modulators," Adv. Opt. Photon. **8**, 200–227 (2016).
13. X. Wang, Z. Nie, Y. Liang, J. Wang, T. Li, and B. Jia, "Recent advances on optical vortex generation," Nanophotonics **7**, 1533–1556 (2018).
14. Y. Shen, X. Wang, Z. Xie, C. Min, X. Fu, Q. Liu, M. Gong, and X. Yuan, "Optical vortices 30 years on: OAM manipulation from topological charge to multiple singularities," Light Sci. Appl. **8**, 90 (2019).
15. M. J. Strain, X. Cai, J. Wang, J. Zhu, D. B. Phillips, L. Chen, M. Lopez-Garcia, J. L. O'Brien, M. G. Thompson, M. Sorel, and S. Yu, "Fast electrical switching of orbital angular momentum modes using ultra-compact integrated vortex emitters," Nat. Commun. **5**, 4856 (2014).
16. Y. Wang, P. Zhao, X. Feng, Y. Xu, K. Cui, F. Liu, W. Zhang, and Y. Huang, "Integrated photonic emitter with a wide switching range of orbital angular momentum modes," Sci. Rep. **6**, 22512 (2016).
17. M. Krenn, M. Huber, R. Fickler, R. Lapkiewicz, S. Ramelow, and A. Zeilinger, "Generation and confirmation of a (100×100)-dimensional entangled quantum system," Proc. Natl. Acad. Sci. USA **111**, 6243–6247 (2014).
18. M. Mafu, A. Dudley, S. Goyal, D. Giovannini, M. McLaren, M. J. Padgett, T. Konrad, F. Petruccione, N. Lutkenhaus, and A. Forbes, "Higher-dimensional orbital-angular-momentum-based quantum key distribution with mutually unbiased bases," Phys. Rev. A **88**, 032305 (2013).
19. M. Krenn, J. Handsteiner, M. Fink, R. Fickler, and A. Zeilinger, "Twisted photon entanglement through turbulent air across Vienna," Proc. Natl. Acad. Sci. USA **112**, 14197–14201 (2015).
20. M. Mirhosseini, O. S. Magaña-Loaiza, M. N. O'Sullivan, B. Rodenburg, M. Malik, M. P. J. Lavery, M. J. Padgett, D. J. Gauthier, and R. W. Boyd, "High-dimensional quantum cryptography with twisted light," New J. Phys. **17**, 033033 (2015).
21. B. Jack, J. Leach, J. Romero, S. Franke-Arnold, M. Ritsch-Marte, S. M. Barnett, and M. J. Padgett, "Holographic ghost imaging and the violation of a Bell inequality," Phys. Rev. Lett. **103**, 083602 (2009).
22. N. Uribe-Patarroyo, A. Fraine, D. S. Simon, O. Minaeva, and A. V. Sergienko, "Object identification using correlated orbital angular momentum states," Phys. Rev. Lett. **110**, 043601 (2013).
23. A. Mair, A. Vaziri, G. Weihs, and A. Zeilinger, "Entanglement of the orbital angular momentum states of photons," Nature **412**, 313–316 (2001).
24. A. Vaziri, G. Weihs, and A. Zeilinger, "Experimental two-photon, three-dimensional entanglement for quantum communication," Phys. Rev. Lett. **89**, 240401 (2002).
25. T. Stav, A. Faerman, E. Maguid, D. Oren, V. Kleiner, E. Hasman, and M. Segev, "Quantum entanglement of the spin and orbital angular momentum of photons using metamaterials," Science **361**, 1101–1104 (2018).
26. R. Fickler, R. Lapkiewicz, W. N. Plick, M. Krenn, C. Schaeff, S. Ramelow, and A. Zeilinger, "Quantum entanglement of high angular momenta," Science **338**, 640–643 (2012).
27. B. Chen, Y. Wei, T. Zhao, S. Liu, R. Su, B. Yao, Y. Yu, J. Liu, and X. Wang, "Bright solid-state sources for single photons with orbital angular momentum," Nat. Nanotechnol. **16**, 302–307 (2021).
28. Q. Zhou, W. Zhang, J. Cheng, Y. Huang, and J. Peng, "Properties of optical fiber based synchronous heralded single photon sources at 1.5 μm," Phys. Lett. A **375**, 2274–2277 (2011).
29. K. Harada, H. Takesue, H. Fukuda, T. Tsuchizawa, T. Watanabe, K. Yamada, Y. Tokura, and S. Itabashi, "Generation of high-purity entangled photon pairs using silicon wire waveguide," Opt. Express **16**, 20368–20373 (2008).
30. G. T. Reed, G. Mashanovich, F. Y. Gardes, and D. J. Thomson, "Silicon optical modulators," Nat. Photonics **4**, 518–526 (2010).
31. D. L. Andrews and M. Babiker, *The Angular Momentum of Light* (Cambridge University, 2012).
32. X. Cai, J. Wang, M. J. Strain, B. Johnson-Morris, J. Zhu, M. Sorel, J. L. O'Brien, M. G. Thompson, and S. Yu, "Integrated compact optical vortex beam emitters," Science **338**, 363–366 (2012).
33. X. Li, J. Chen, P. Voss, J. Sharping, and P. Kumar, "All-fiber photon-pair source for quantum communications: improved generation of correlated photons," Opt. Express **12**, 3737–3744 (2004).
34. J. E. Sharping, K. F. Lee, M. A. Foster, A. C. Turner, B. S. Schmidt, M. Lipson, A. L. Gaeta, and P. Kumar, "Generation of correlated photons in nanoscale silicon waveguides," Opt. Express **14**, 12388–12393 (2006).
35. H. Takesue and K. Inoue, "1.5-μm band quantum-correlated photon pair generation in dispersion-shifted fiber: suppression of noise photons by cooling fiber," Opt. Express **13**, 7832–7839 (2005).
36. S. Clemmen, K. P. Huy, W. Bogaerts, R. G. Baets, Ph. Emplit, and S. Massar, "Continuous wave photon pair generation in silicon-on-insulator waveguides and ring resonators," Opt. Express **17**, 16558–16570 (2009).